



# SN 2022jli: A Type Ic Supernova with Periodic Modulation of Its Light Curve and an Unusually Long Rise

T. Moore<sup>1</sup> , S. J. Smartt<sup>1,2</sup> , M. Nicholl<sup>1</sup> , S. Srivastav<sup>1</sup> , H. F. Stevance<sup>2,3</sup> , D. B. Jess<sup>1,4</sup> , S. D. T. Grant<sup>1</sup> , M. D. Fulton<sup>1</sup> , L. Rhodes<sup>2</sup> , S. A. Sim<sup>1</sup> , R. Hirai<sup>5,6</sup> , P. Podsiadlowski<sup>7</sup> , J. P. Anderson<sup>8,9</sup> , C. Ashall<sup>10</sup> , W. Bate<sup>1</sup> , R. Fender<sup>2</sup> , C. P. Gutiérrez<sup>11,12</sup> , D. A. Howell<sup>13,14</sup> , M. E. Huber<sup>15</sup> , C. Inerra<sup>16</sup> , G. Leloudas<sup>17</sup> , L. A. G. Monard<sup>18</sup>, T. E. Müller-Bravo<sup>11,12</sup> , B. J. Shappee<sup>15</sup> , K. W. Smith<sup>1</sup> , G. Terreran<sup>13</sup> , J. Tonry<sup>15</sup> , M. A. Tucker<sup>19,20,21</sup> , D. R. Young<sup>1</sup> , A. Aamer<sup>1,22</sup> , T.-W. Chen<sup>23</sup> , F. Ragosta<sup>24,25</sup> , L. Galbany<sup>11,12</sup> , M. Gromadzki<sup>26</sup> , L. Harvey<sup>27</sup> , P. Hoefflich<sup>28</sup> , C. McCully<sup>13</sup> , M. Newsome<sup>13,14</sup> , E. P. Gonzalez<sup>13,14</sup> , C. Pellegrino<sup>13,14</sup> , P. Ramsden<sup>29,30</sup> , M. Pérez-Torres<sup>31,32</sup> , E. J. Ridley<sup>22,33</sup> , X. Sheng<sup>1</sup> , and J. Weston<sup>1</sup>

<sup>1</sup> Astrophysics Research Centre, School of Mathematics and Physics, Queen's University Belfast, BT7 1NN, UK; [tmoore11@qub.ac.uk](mailto:tmoore11@qub.ac.uk)

<sup>2</sup> Department of Physics, University of Oxford, Denys Wilkinson Building, Keble Road, Oxford OX1 3RH, UK

<sup>3</sup> Department of Physics, The University of Auckland, Private Bag 92019, Auckland, New Zealand

<sup>4</sup> Department of Physics and Astronomy, California State University Northridge, Northridge, CA 91330, USA

<sup>5</sup> OzGrav: The Australian Research Council Centre of Excellence for Gravitational Wave Discovery, Clayton, VIC 3800, Australia

<sup>6</sup> School of Physics and Astronomy, Monash University, VIC 3800, Australia

<sup>7</sup> University of Oxford, St Edmund Hall, Oxford OX1 4AR, UK

<sup>8</sup> European Southern Observatory, Alonso de Córdova 3107, Casilla 19, Santiago, Chile

<sup>9</sup> Millennium Institute of Astrophysics MAS, Nuncio Monsenor Sotero Sanz 100, Off. 104, Providencia, Santiago, Chile

<sup>10</sup> Department of Physics, Virginia Tech, Blacksburg, VA 24061, USA

<sup>11</sup> Institut d'Estudis Espacials de Catalunya (IEEC), E-08034 Barcelona, Spain

<sup>12</sup> Institute of Space Sciences (ICE, CSIC), Campus UAB, Carrer de Can Magrans, s/n, E-08193 Barcelona, Spain

<sup>13</sup> Las Cumbres Observatory, 6740 Cortona Drive, Suite 102, Goleta, CA 93117-5575, USA

<sup>14</sup> Department of Physics, University of California, Santa Barbara, CA 93106-9530, USA

<sup>15</sup> Institute for Astronomy, University of Hawai'i, 2680 Woodlawn Drive, Honolulu, HI 96822, USA

<sup>16</sup> Cardiff Hub for Astrophysics Research and Technology, School of Physics & Astronomy, Cardiff University, Queens Buildings, The Parade, Cardiff, CF24 3AA, UK

<sup>17</sup> DTU Space, National Space Institute, Technical University of Denmark, Elektrovej 327, DK-2800 Kgs. Lyngby, Denmark

<sup>18</sup> Kleinkaroo Observatory, Calitzdorp, Western Cape, South Africa

<sup>19</sup> Department of Astronomy, The Ohio State University, 140 West 18th Avenue, Columbus, OH, USA

<sup>20</sup> Department of Physics, The Ohio State University, 191 West Woodruff Avenue, Columbus, OH, USA

<sup>21</sup> Center for Cosmology and Astroparticle Physics, The Ohio State University, 191 West Woodruff Avenue, Columbus, OH, USA

<sup>22</sup> Institute for Gravitational Wave Astronomy and School of Physics and Astronomy, University of Birmingham, Birmingham B15 2TT, UK

<sup>23</sup> Graduate Institute of Astronomy, National Central University, 300 Jhongda Road, 32001 Jhongli, Taiwan

<sup>24</sup> INAF, Osservatorio Astronomico di Roma, via Frascati 33, I-00078 Monte Porzio Catone (RM), Italy

<sup>25</sup> Space Science Data Center—ASI, Via del Politecnico SNC, I-00133 Roma, Italy

<sup>26</sup> Astronomical Observatory, University of Warsaw, Al. Ujazdowskie 4, 00-478 Warszawa, Poland

<sup>27</sup> School of Physics, Trinity College Dublin, The University of Dublin, Dublin 2, D02 PN40, Ireland

<sup>28</sup> Department of Physics, Florida State University, 77 Chieftan Way, Tallahassee, FL 32306, USA

<sup>29</sup> School of Physics and Astronomy, University of Birmingham, Birmingham B15 2TT, UK

<sup>30</sup> Institute for Gravitational Wave Astronomy, University of Birmingham, Birmingham B15 2TT, UK

<sup>31</sup> Instituto de Astrofísica de Andalucía (IAA-CSIC), Glorieta de la Astronomía s/n, E-18008 Granada, Spain

<sup>32</sup> School of Sciences, European University Cyprus, Diogenes street, Engomi, 1516 Nicosia, Cyprus

<sup>33</sup> School of Physics and Astronomy, University of Birmingham, Edgbaston, B15 2TT, UK

Received 2023 August 14; revised 2023 September 12; accepted 2023 September 16; published 2023 October 13

## Abstract

We present multiwavelength photometry and spectroscopy of SN 2022jli, an unprecedented Type Ic supernova discovered in the galaxy NGC 157 at a distance of  $\approx 23$  Mpc. The multiband light curves reveal many remarkable characteristics. Peaking at a magnitude of  $g = 15.11 \pm 0.02$ , the high-cadence photometry reveals periodic undulations of  $12.5 \pm 0.2$  days superimposed on the 200-day supernova decline. This periodicity is observed in the light curves from nine separate filter and instrument configurations with peak-to-peak amplitudes of  $\simeq 0.1$  mag. This is the first time that repeated periodic oscillations, over many cycles, have been detected in a supernova light curve. SN 2022jli also displays an extreme early excess that fades over  $\approx 25$  days, followed by a rise to a peak luminosity of  $L_{\text{opt}} = 10^{42.1}$  erg s<sup>-1</sup>. Although the exact explosion epoch is not constrained by data, the time from explosion to maximum light is  $\gtrsim 59$  days. The luminosity can be explained by a large ejecta mass ( $M_{\text{ej}} \approx 12 \pm 6 M_{\odot}$ ) powered by <sup>56</sup>Ni, but we find it difficult to quantitatively model the early excess with circumstellar interaction and cooling. Collision between the supernova ejecta and a binary companion is a possible source of this emission. We discuss the origin of the periodic variability in the light curve, including interaction of the SN ejecta with nested shells of circumstellar matter and neutron stars colliding with binary companions.



Original content from this work may be used under the terms of the [Creative Commons Attribution 4.0 licence](https://creativecommons.org/licenses/by/4.0/). Any further distribution of this work must maintain attribution to the author(s) and the title of the work, journal citation and DOI.

*Unified Astronomy Thesaurus concepts:* [Transient sources \(1851\)](#); [Supernovae \(1668\)](#); [Core-collapse supernovae \(304\)](#); [Type Ic supernovae \(1730\)](#)

*Supporting material:* data behind figure, tar.gz file

## 1. Introduction

Stars with zero-age main-sequence masses ( $M_{\text{ZAMS}}$ ) greater than  $8 M_{\odot}$  end their lives as core-collapse supernovae (CCSNe; Smartt 2009; Langer 2012), producing a diverse range of transients (e.g., Gal-Yam 2017; Modjaz et al. 2019). The variety in the observable properties of these SNe is thought to be dependent on the initial mass, metallicity, binarity, and mass-loss history of the progenitor star. Hydrogen-poor CCSNe are referred to as stripped-envelope SNe (SESNe) owing to significant mass loss of the progenitor, removing hydrogen, and in some cases helium, from the stellar envelope. SESNe classified as Type Ic do not show hydrogen or helium in their optical spectra, although the extent of helium stripping is still uncertain (Hachinger et al. 2012; Williamson et al. 2021). Envelope stripping can occur through strong stellar line-driven winds (e.g., Vink & de Koter 2005; Shenar et al. 2020) or interaction with a binary companion (Podsiadlowski et al. 1992).

Evidence for periodicity has been searched for in SN light curves. Nicholl et al. (2016) investigated the undulations in the superluminous SN 2015bn but were limited by the duration of their time series and could not reliably identify periodicity. West et al. (2023) suggested a repeating pattern of  $32 \pm 6$  days in the declining light curve of SN 2020qlb (an explosion somewhat similar to SN 2015bn). However, insufficient cycles were observed to perform robust statistical checks for periodicity. Martin et al. (2015) and Fraser et al. (2013) suggested a periodicity in the optical light curve of SN 2009ip, but Fraser et al. (2015) subsequently found no evidence for the periodicity in extensive  $R$ -band data. The light curve of the luminous, fast optical transient AT 2018cow was subject to periodicity searches, and while none were found in the optical, marginal evidence for periodicity in the variable X-ray light curve was suggested (Rivera Sandoval et al. 2018; Kuin et al. 2019; Margutti et al. 2019). Perhaps the most promising detection of periodicity in SN emission is in the radio light curves of SN 1979C (Weiler et al. 1992) and SN 2001ig (Ryder et al. 2004), which have been attributed to fluctuations in the density of the circumstellar medium (CSM) produced by binary stellar wind interactions.

In this paper we present an extensive follow-up campaign of the Type Ic SN 2022jli from  $\sim -50$  to  $+200$  days relative to maximum light. SN 2022jli presents an unusually long-lived, luminous early excess followed by a long rise time and slow spectroscopic evolution. The extensive, almost daily, photometric coverage of this bright SN for 200 days after peak indicates a periodic variability ( $P = 12.5 \pm 0.2$  days) observed in multiple bands and instruments, with amplitude of order 1% of the peak bolometric luminosity of the SN.

## 2. Discovery and Classification

Libert Monard discovered a transient in NGC 157 from Kleinkaroo Observatory and submitted the discovery report on the Transient Name Server (TNS) as AT 2022jli on 2022 May 5.17 UT at an unfiltered magnitude  $\simeq 14$  mag (Monard 2022). With the ATLAS survey (Tonry et al. 2018b; Smith et al. 2020), we independently detected the object (internal name ATLAS22oat) on 2022 May 16.41 (at  $o = 14.3$  mag). The original TNS

Discovery Report of Monard (2022) registered the object with an astrometric error of  $14''$ ,<sup>34</sup> and our ATLAS transient server (Smith et al. 2020), which dynamically links to TNS discoveries, did not associate the two sources. The ATLAS-automated TNS registration triggered a new source ( $\alpha = 8^{\circ}69038$   $\delta = -8^{\circ}38668$ ), a discovery report, and name (AT 2022jzy). To prevent confusion, AT 2022jzy was manually removed entirely from the TNS records, and the original incorrect coordinates of AT 2022jli were replaced with those from ATLAS while preserving L. Monard’s discovery credit (O. Yaron, private communication). A low-resolution ( $R = 100$ ) spectrum from a 0.35 m telescope (Grzegorzec 2022) indicated a likely Type Ic. This classification was confirmed (Cosentino et al. 2022) by the extended Public ESO Spectroscopic Survey of Transient Objects (ePESSTO+; Smartt et al. 2015).

The SN is offset by  $35''2$  N and  $15''88$  W from the center of its host galaxy NGC 157, which has a redshift of  $z = 0.0055$ . The kinematic distance on the NASA/IPAC Extragalactic Database (NED), from the recessional velocity (corrected for Virgo infall and assuming  $H_0 = 73 \text{ km s}^{-1} \text{ Mpc}^{-1}$ ), is  $D = 23 \pm 2$  Mpc. Distance estimates from the Tully–Fisher and Sosies methods (e.g., Terry et al. 2002; Tully et al. 2013) have a large range from 11 to 29 Mpc, and we adopt the kinematic distance  $D = 23 \pm 2$  Mpc throughout the rest of this paper. The foreground Milky Way reddening is  $A_V = 0.1186$  (Schlafly & Finkbeiner 2011), and given the position of SN 2022jli, some internal host extinction is likely present. We do not account for possible host extinction, but this is likely to be low owing to the lack of narrow Na I D absorption in the spectra (Poznanski et al. 2012), and our main results are not sensitive to this choice. The spectroscopy and photometry presented in this paper have been corrected for foreground galactic extinction, and the spectra have been shifted into the rest frame. We note that NGC 157 also hosted the Type Ic SN 2009em (Monard 2009).

## 3. Observations

### 3.1. Imaging and Photometry

The first observations of SN 2022jli were reported to the TNS by L. Monard (Monard 2022). To our knowledge there are no pre-explosion nondetections available, as the object had just emerged from solar conjunction. Monard reported four epochs of unfiltered CCD photometry from observations taken at the Kleinkaroo Observatory between 2022 May 5 (MJD 59704) and 2022 May 22 UT (MJD 59721).

The Asteroid Terrestrial-impact Last Alert System (ATLAS; Tonry et al. 2018b) began observing at the position of SN 2022jli on 2022 May 16 (MJD 59715) in normal survey operations. ATLAS is a quadruple 0.5 m telescope system using broad orange ( $o$ , 5600–8200 Å) and cyan ( $c$ , 4200–6500 Å) filters. The combined four-telescope system surveys the observable sky to a typical  $5\sigma$  depth of  $\sim 19$  mag and a cadence of 1–2 days. ATLAS photometry and astrometry are calibrated with the all-sky reference catalog sky (refcat2;

<sup>34</sup> L. Monard corrected this a day later in the TNS Comment for AT 2022jli, but the TNS database coordinates remained in error.

Tonry et al. 2018a). ATLAS photometry for SN 2022jli was obtained by forcing photometry at the location using the ATLAS forced photometry server (Shingles et al. 2021) and adopting a  $3\sigma$  clipped nightly mean.

The Zwicky Transient Facility (ZTF; Bellm et al. 2019) observed the field beginning on 2022 July 03 UT (MJD 59763), giving the object the internal name ZTF22aapubuy. ZTF photometry in both  $g$  and  $r$  bands was obtained from the ZTF public stream using the Lasair<sup>35</sup> broker (Smith et al. 2019).

Photometry from ASAS-SN (Shappee et al. 2014) beginning on 2022 May 09 UT (MJD 59708) was obtained using the ASAS-SN Sky Patrol website<sup>36</sup> (Kochanek et al. 2017). We adopt a cutoff MJD of 59762, after which we do not include ASAS-SN  $g$ -band photometry in favor of higher signal-to-noise ratio ZTF  $g$  band.

We triggered follow-up photometric observations of SN 2022jli using the IO:O camera at the 2 m Liverpool Telescope (LT; Steele et al. 2004). Using the LT, we obtained six epochs of  $ugriz$ -band observations and an additional  $griz$ -band observation between MJD 59817 and 59894.

The  $griBV$ -band photometry was obtained through the Global Supernova Project using the 1 m Las Cumbres Observatory (LCO; Brown et al. 2013). Additional  $V$ -band observations were recovered from acquisition images taken with the ESO Faint Object Spectrograph and Camera version 2 (EFOSC2; Snodgrass et al. 2008) on the ESO 3.58 m New Technology Telescope (NTT; Wilson 1983) during spectroscopic follow-up by PESSTO (Smartt et al. 2015).

All CCD reductions were performed using instrument specific pipelines. Photometric measurements for the LCO 1 m, EFOSC2, and  $griz$  LT-IO:O data were made using AUTOPHOT (Brennan & Fraser 2022) without host subtraction. Photometry in  $griz$  bands was calibrated against Pan-STARRS field stars (Flewelling et al. 2020), and  $BV$ -band photometry was calibrated using the APASS catalog (Henden et al. 2016). LT  $u$ -band measurements were performed using the PSF package<sup>37</sup> (Nicholl et al. 2023) and calibrated against the Sloan Digital Sky Survey (SDSS; Alam et al. 2015) catalog.

The Gaia satellite (Gaia Collaboration et al. 2016), operated by the European Space Agency (ESA), observed SN 2022jli (internal name Gaia22cbu) between 2022 May 11 (MJD 59710) and 2022 June 30 UT (MJD 59760). The Gaia Science Alerts Project (Hodgkin et al. 2021) reported three epochs of  $G$ -band photometry.<sup>38</sup> We assume a pessimistic Gaia photometric uncertainty of 0.1 mag.

Ultraviolet (UV) and optical photometry of SN 2022jli was performed with the Ultra-Violet and Optical Telescope (UVOT; Roming et al. 2005) on board the Neil Gehrels Swift Observatory (Swift; Gehrels et al. 2004). Swift observed the field 13 times between 2022 August 17 (MJD 59808) and 2022 December 27 (MJD 59940) in the  $U$ ,  $B$ ,  $V$ ,  $UVW1$ ,  $UVM2$ , and  $UVW2$  bands. The images in each filter were co-added, and SN magnitudes were extracted using standard tasks within the HEASOFT<sup>39</sup> package. A small aperture of  $3''$  was chosen, and an aperture correction was applied, following Brown et al. (2009). Without template subtraction, most  $UVW1$ ,  $UVM2$ , and  $UVW2$  exposures were nondetections. Keeping only detections

greater than the limiting magnitude, we retain only one epoch of  $UVM2$  photometry but retain most observations in the  $UBV$  bands. The extinction-corrected light curve of SN 2022jli is shown in Figure 1.

### 3.2. Radio Observation

We obtained a single radio observation at the position of SN 2022jli on 2022 September 19, starting at 22:15 UT with the enhanced Multi-Element Remotely Linked Interferometer Network (e-Merlin; DD14001; PI: Rhodes). Observations were obtained at a central frequency of 5.08 GHz with a bandwidth of 512 MHz. The observation consisted of 6-minute scans of the target interleaved with 2-minute scans on the phase calibrator (J0039–0942). The observation ended with a scan of the flux calibrator (J1331+3030) and the bandpass calibrator (J1407+2827). The data were processed using the e-MERLIN custom CASA-based pipeline (Version 5.8, Moldon 2021).

The pipeline averages the data in both time and frequency space, flags the data for radio frequency interference, performs bandpass and complex gain calibration, and splits out the calibrated target field. We performed some further flagging and imaged the data within CASA. During the observation, two of the six antennas dropped out, which impacted the quality of the final image. We did not detect any radio emission at the position of SN 2022jli, and we measure a final rms noise of about  $52 \mu\text{Jy beam}^{-1}$  (and a  $3\sigma$  upper limit of  $156 \mu\text{Jy beam}^{-1}$ ).

### 3.3. Spectroscopy

We present our spectra spanning three epochs,  $-39$  days to  $+47$  days with respect to  $g$ -band maximum, and also show the low-resolution spectrum of Grzegorzec (2022) from the TNS (additional spectra will be presented in a separate publication). Foreground Galactic reddening was corrected using the `dust_extinction` package of `Astropy` following the Fitzpatrick (1999) reddening law. All spectra presented in this work will be made available via the WISeREP repository (Yaron & Gal-Yam 2012).

Follow-up spectroscopy was acquired using the EFOSC2 at the 3.58m NTT (Snodgrass et al. 2008) at two epochs through ePESSTO+. The first EFOSC2 spectrum was taken on 2022 May 24.42 UT (MJD = 59723.42), and our final spectrum was taken on MJD = 59811.15. The EFOSC2 grism used for the spectral sequence was Gr#13 (3685–9315 Å). Data reductions were performed using the PESSTO pipeline, which includes flat-fielding, bias-subtraction, wavelength and telluric correction, and flux calibration as described by Smartt et al. (2015).

One epoch from the University of Hawaii 2.2 m telescope was obtained on 2022 July 24.62 (MJD 59784.62) using SNIFS (Lantz et al. 2004). The SNIFS spectrum was reduced using the Spectroscopic Classification of Astronomical Transients (SCAT) survey pipeline (Tucker et al. 2022).

The extinction-corrected spectra are shown in Figure 2.

## 4. Analysis

### 4.1. Light Curve

SN 2022jli fades for  $\sim 25$  days after discovery in the  $go$  bands; using a linear fit, we measure a decline rate of  $\sim 5$  mag  $(100 \text{ days})^{-1}$ , which is incompatible with  $^{56}\text{Co}$  decay. This early decline is not well sampled with low-cadence coverage from only ASAS-SN ( $g$ ), ATLAS ( $o$ ), Gaia, and a single  $V$ -

<sup>35</sup> <https://lasair-ztf.lsst.ac.uk/object/ZTF22aapubuy/>

<sup>36</sup> <https://asas-sn.osu.edu>

<sup>37</sup> <http://github.com/mnicholl/photometry-sans-frustration>

<sup>38</sup> <http://gsaweb.ast.cam.ac.uk/alerts/alert/Gaia22cbu/>

<sup>39</sup> <https://heasarc.gsfc.nasa.gov/lheasoft>

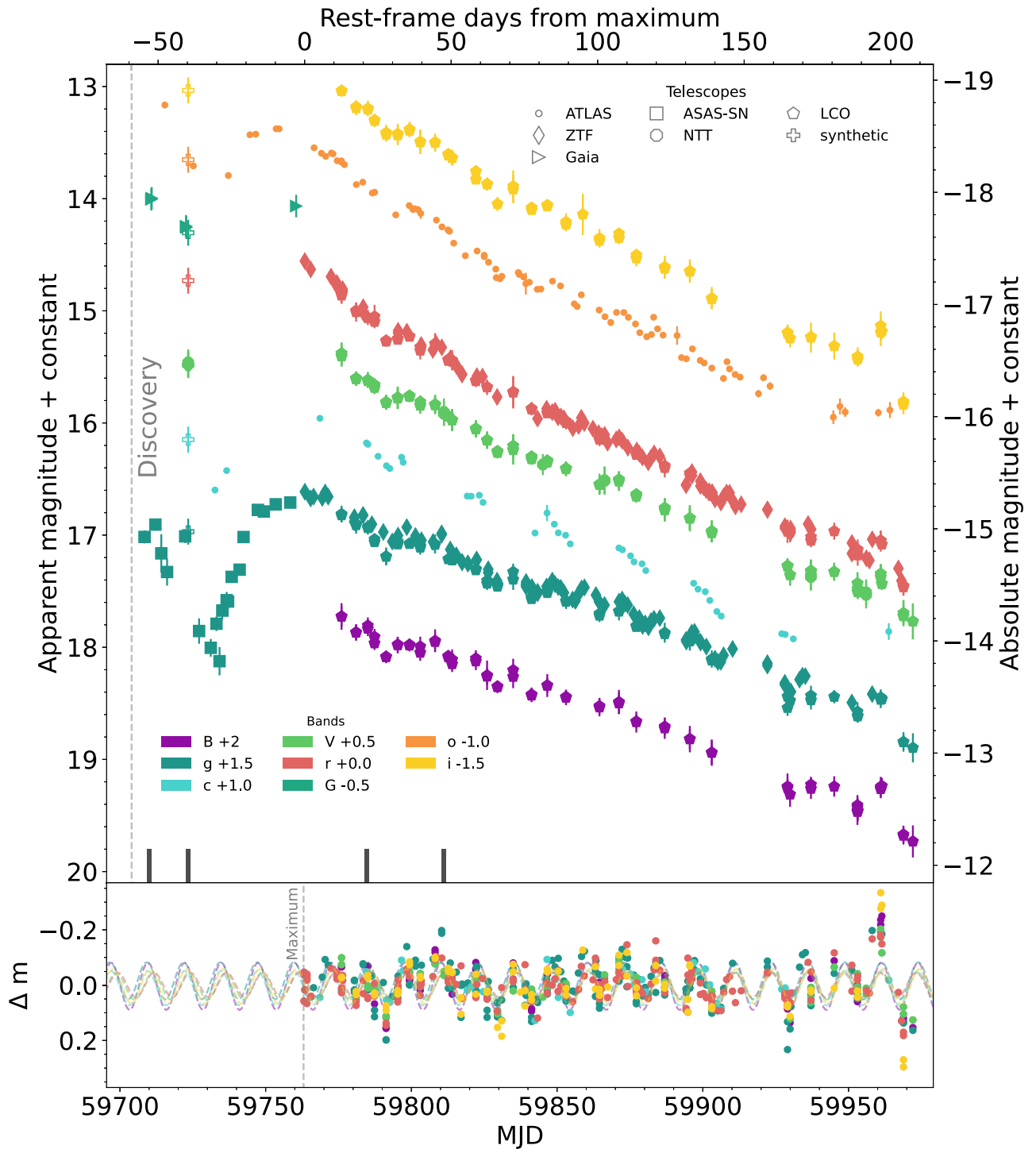


**Figure 1.** Top: multicolor extinction-corrected light curves of SN 2022jli including photometric errors. Black lines along the bottom of the plot indicate spectroscopic observations. Open symbols are synthetic photometry performed on the EFOSC2 spectrum. Bottom: light curves after detrending with a second-degree polynomial fit including only the region after maximum light (vertical dashed line). Overplotted for each band are the best-fit sinusoids produced in the GLS analysis (Section 4.2). We retain the colors from the top panel and remove variation of point shape and do not include photometric errors for visual clarity, including only observations after MJD 59750.

(The data used to create this figure are available.)

band observation from the NTT. The light curve begins to rise after MJD 59734, reaching maximum light on MJD 59763, indicating that the main peak is at  $\sim 59$  rest-frame days from discovery. SN 2022jli exhibits a significantly longer rise to maximum light than literature samples of SESNe (Prentice et al. 2019), comparable to a small subset of slowly evolving

Type Ibc SNe (e.g., Anupama et al. 2005; Lyman et al. 2016; Taddia et al. 2016, 2018; Karamahmetoglu et al. 2023). The SN eventually fades in the optical at a rate of  $\sim 1$  mag  $(100 \text{ days})^{-1}$ , which is compatible with  $^{56}\text{Co}$  decay, suggesting a radioactively powered main peak (Woosley et al. 1989). The  $r$  band declines  $0.4$  mag  $(100 \text{ days})^{-1}$  faster than the  $g$

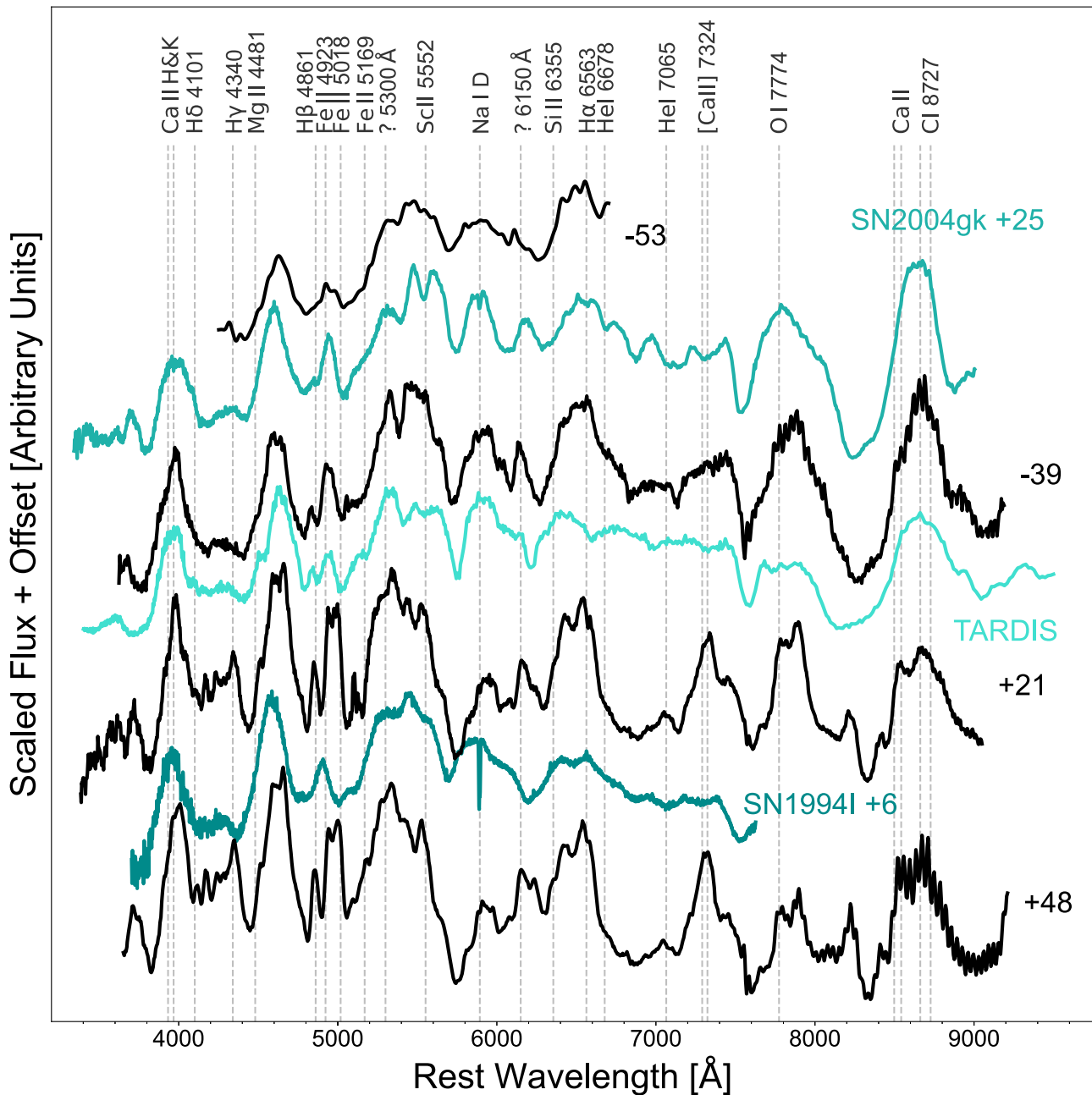


**Figure 2.** Spectroscopic follow-up observation of SN 2022jli. Spectra are labeled by time since maximum light in the rest frame. Common SN lines are marked as vertical lines corresponding to the rest wavelengths. We include here the Grzegorzec (2022) classification spectrum. A TARDIS (Kerzendorf & Sim 2014) model of H- and He-free material is also included. Spectra for the Type Ic SNe SN 2004gk (Shivvers et al. 2019) and SN 1994I (Modjaz et al. 2014) were obtained from WISeREP (Yaron & Gal-Yam 2012).

band, showing an unusual evolution toward bluer colors in  $g - r$  over time. The double-peaked early light curve indicates that  $^{56}\text{Ni}$  decay cannot account for the full structure of the light curve.

As the light curve slowly fades from peak, the extensive high-cadence photometry of SN 2022jli captures clear undulations in the photometry. The undulations are visible in multiple bands ( $B$  to  $i$ ) and across different telescope and instrument combinations, indicating that this is neither an instrumental nor a calibration effect. We subtract the SN continuum and reveal these undulations more clearly in the bottom panel of Figure 1. We identify repeating bumps with a consistent timescale for all filters and discuss this in detail in Section 4.2.

During the initial decline, we observe an increase in the ASAS-SN  $g$ -band photometry on MJD 59722.37. Seeking to

confirm the validity of this observation, we perform synthetic photometry on the EFOSC2 spectrum taken on MJD 59723.42, which was calibrated to the  $V$ -band acquisition image. We include the synthetic photometry in Figure 1; the errors on the points are consistent with the ASAS-SN  $g$ -band photometry and other contemporary photometric observations in  $G$  and  $o$  bands. We interpret this epoch as a short-lived, luminous episode during the initial excess.

#### 4.1.1. Bolometric Light Curve

We compute a pseudobolometric light curve by integrating under the  $BgcVrGoiz$ -band observations using the publicly available code SUPERBOL (Nicholl 2018). From our

bolometric light curve we measure a peak luminosity  $L_{\text{opt}} = 10^{42.08 \pm 0.04} \text{ erg s}^{-1}$ , which is within the typical range of SESNe found by Prentice et al. (2019). The total integrated luminosity (across the wavelength range covered by our filters) is  $E_{\text{opt}} \approx 2.5 \times 10^{49} \text{ ergs}$ .

We compare the (pseudo)bolometric light curve to other SNe, including normal SESNe and those with double-peaked light curves, in Figure 3. SN 2022jli exceeds the peak brightness of the Type Ic SN 2007gr (Hunter et al. 2009), the Type Ib SN 2008D (Soderberg et al. 2008; Modjaz et al. 2009), and the relatively faint Type Ib SN 2007Y (Stritzinger et al. 2009), showing a significantly more luminous broad peak and slower decay. SN 2007gr and SN 2007Y both display a monotonic rise and smooth decline, typical of a normal Type Ibc SN, unlike the double-peaked structured light curve of SN 2022jli. The overall shape of the light curve resembles the unusual Type Ic iPTF15dtg (Taddia et al. 2016). Both SNe have a fast-declining early excess with a broad persistent maximum. SN 2005bf (Anupama et al. 2005) has an early peak and broad maximum but is significantly more luminous than SN 2022jli and declines significantly faster.

#### 4.1.2. Light-curve Modeling

We model the light curve using simple models to derive a representative ejecta mass estimate for SN 2022jli using the Modular Open Source Fitter for Transients (MOSFiT; Guillochon et al. 2018). MOSFiT is a publicly available code that we use to fit semianalytic models to the multiband observed light curves of SN 2022jli. We use two models, one where we model only the broad “main” peak assuming radioactive decay of  $^{56}\text{Ni}$  as the only energy source (Arnett 1982; Nadyozhin 1994), and another where we fit the full light curve interpreting the initial excess as shock cooling emission (SCE) from interaction with a CSM and a subsequent radioactively powered “main” peak (Chatzopoulos et al. 2013). All model fitting was performed using the dynamic nested sampler DYNESTY package (Speagle 2020) option in MOSFiT.

The bottom panel of Figure 3 shows the  $^{56}\text{Ni}$ -only model fit to SN 2022jli. To construct this model, we used the nickel-driven explosion model built into MOSFiT (Nadyozhin 1994), omitting any data during the early excess (before MJD 59732). We modify the priors of the model to require the explosion time to be before discovery, i.e.,  $\text{MJD}_{\text{explosion}} < \text{MJD}_{\text{discovery}}$ ; The opacity was fixed at  $\kappa = 0.1 \text{ cm}^2 \text{ g}^{-1}$  and  $\kappa_{\gamma} = 0.027 \text{ cm}^2 \text{ g}^{-1}$ . With no prior on ejecta velocity, the data require  $v_{\text{ej}} \approx 2500 \text{ km s}^{-1}$  and  $M_{\text{ej}} \approx 4 M_{\odot}$ ; this velocity is much lower than the measurements of the Fe II lines in the spectra (see Section 4.3). The posterior distribution for this fit is included in the Appendix (Figure 5).

This model reproduces the maximum luminosity for the  $g$  and  $c$  bands but fits poorly to the redder bands, underestimating the flux particularly in the  $o$  and  $i$  bands. This simple model also fails to reproduce the fast  $g$ -band rise after the light-curve dip and the  $o$ -band peak luminosity. Color differences between the model light curve and the observed data are likely due to the blackbody assumption made by MOSFiT, as the true spectrum is dominated by strong emission and absorption lines by the time of maximum light. Further detailed modeling is warranted using more sophisticated techniques, which is beyond the scope of this work. For comparison, we perform an additional Arnett model (Arnett 1982) fit to the bolometric

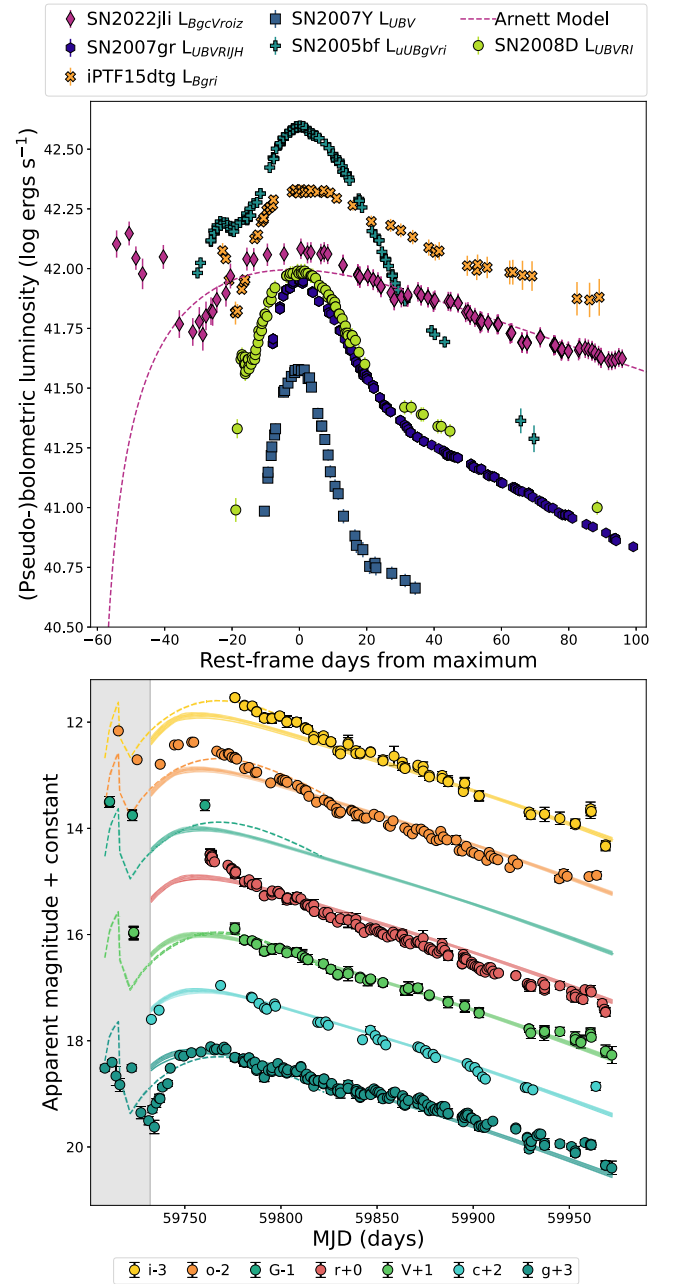


**Figure 3.** Top: pseudobolometric light-curve comparison of SN 2022jli and other SNe with prominent bumps and well-studied Type Ibc SNe. The bolometric light curves of the Type Ic SN 2007gr (Hunter et al. 2009), Type Ib SN 2007Y (Stritzinger et al. 2009), Type Ic iPTF15dtg (Taddia et al. 2016), Type Ib SN 2008D (Soderberg et al. 2008; Modjaz et al. 2009); pseudobolometric light curve calculated in Nicholl et al. 2015), and Type Ib/c SN 2005bf (Anupama et al. 2005) were also constructed using SUPERBOL. The dashed line represents an Arnett model (Arnett 1982) fit to the SN 2022jli light curve after MJD 59732. Bottom: MOSFiT (Guillochon et al. 2018) multiband fit results for a  $^{56}\text{Ni}$  explosion model (solid lines). We include the best scoring realization from a CSM +  $^{56}\text{Ni}$  model fit to the first 110 days of SN 2022jli as a dashed line.

light curve with a  $\chi^2$  fitting approach. Fixing  $\kappa = 0.1 \text{ cm}^2 \text{ g}^{-1}$  and  $v_{\text{ej}} \approx 3000 \text{ km s}^{-1}$ , we require  $M_{\text{ej}} \approx 6 M_{\odot}$ , which is in agreement with the results from MOSFiT. This fit is included in Figure 3.

To gauge the systematic modeling uncertainties within MOSFiT, we run the same nickel-driven model for the main peak with a range of  $v_{\text{ej}}$  to determine a probable range of  $M_{\text{ej}}$ . A

fixed ejecta velocity of  $v_{\text{ej}} = 3500 \text{ km s}^{-1}$  requires  $M_{\text{ej}} \approx 7 M_{\odot}$ ,  $v_{\text{ej}} = 6000 \text{ km s}^{-1}$  requires  $M_{\text{ej}} \approx 18 M_{\odot}$ , and  $v_{\text{ej}} = 7000 \text{ km s}^{-1}$  forces  $M_{\text{ej}} \approx 21 M_{\odot}$ . With no pre-explosion nondetections available to constrain the explosion time and large systematic errors on the model, we adopt an indicative mass range for SN 2022jli of  $M_{\text{ej}} \approx 12 \pm 6 M_{\odot}$ .

In the second scenario we consider the contribution of SCE following shock breakout of the ejecta through a dense CSM using the  $^{56}\text{Ni} + \text{CSM}$  (CSMNI) model (Chatzopoulos 2013; Villar et al. 2017; Jiang et al. 2020). SCE is a natural interpretation for a fast-declining excess shortly after explosion and is now regularly detected for a range of SN subtypes. The same assumptions are made for the opacities as before, but the explosion time is left as a free parameter of the fit. We modify the code so that the interaction begins when the ejected material reaches the inner radius of the CSM at  $R_0$ . Our results indicate a CSM radius  $R_0 \sim 1 \text{ au}$ ,  $M_{\text{ej}} \sim 20 M_{\odot}$ ,  $M_{\text{CSM}} \sim 26 M_{\odot}$ , and  $f_{\text{Ni}} \sim 0.01$  for the early excess to be powered by CSM interaction. Our model (fit to the first 110 days) results in a poor match to the observed data, particularly the colors of the early excess, and requires physically improbable parameters; this model is shown in Figure 3.

Although the Chatzopoulos et al. (2013) model implemented in MOSFiT is relatively simple, the very large ejecta masses required imply that this scenario is physically unlikely. We return to this point in Section 5.2. We also emphasize that there is no robust measurement of explosion time to constrain the model since the earliest epoch from the Monard observations is after the SN appeared from solar conjunction.

A long rise time (exceeding 30 days) is a rare occurrence for Type Ibc SNe (Lyman et al. 2016): long-duration light curves with rise times similar to SN 2022jli arise from only  $\sim 6\%$ – $10\%$  of SNe Ibc in a bias-corrected sample (Karamahmetoglu et al. 2023). We estimate that  $M_{\text{ej}} = 12 \pm 6 M_{\odot}$  is required to provide the long rise to maximum light. An ejecta mass this extreme is rare and points to a high-mass progenitor star.

#### 4.2. Periodic Variability

The declining light curve (Figure 1) shows  $\sim 0.05 \text{ mag}$  undulations, which are present across all bands and appear to repeat with a regular amplitude and period. To search for and quantify any periodicity, we first removed the decline signature from the light curve. From the post-peak light-curve data (MJD  $> 59760$ ), we produced a residual light curve in each band by fitting and subtracting a fourth-order polynomial fit (the lowest order that removes the SN decline) between MJD 59760 and the end of the time series for each band. We applied this method to each of the *BgcVroi* bands independently and include the results in the bottom panel of Figure 1. The residual light curves show consistent oscillations over time across all bands. The periodicity in each of the residual light curves was quantified by computing a periodogram using a generalized Lomb–Scargle (GLS) method (Zechmeister & Kürster 2009). The periodograms for each band and a phase-folded light curve are shown in Figure 4.

We find that the undulations have a dominant frequency of  $\sim 0.08 \text{ day}^{-1}$  (or a period of  $\sim 12.5 \text{ days}$ ), where significant power is observed across the period range of 12–13 days, which is safely below the  $\Delta t/3$  cutoff adopted by Martin et al. (2015) and Nicholl et al. (2016), where  $\Delta t$  is the length of the time series. The maximum GLS power in this region exceeds

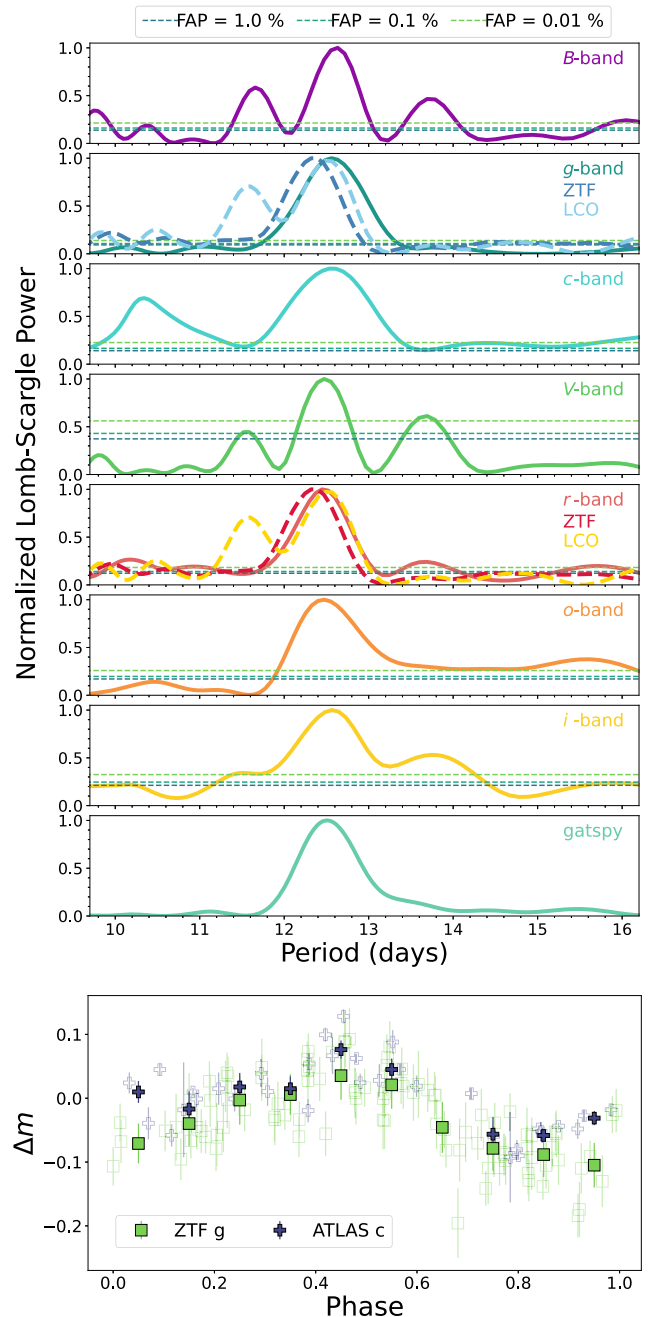


**Figure 4.** Top: GLS periodograms from *BgcVroi* bands, where dashed horizontal lines correspond to the 1%, 0.1%, and 0.01% FAP levels. The bottom panel shows a Lomb–Scargle periodogram generated from all bands simultaneously using *gatspy*. For the *gr* bands additional periodograms are computed using only LCO and ZTF photometry; the associated FAP levels for these periodograms are not plotted. All periodograms regardless of band or telescope–instrument combination show a significant power at  $\sim 12.5$  days. Bottom: binned phase-folded ZTF *g*-band and ATLAS *c*-band light curve. Each band has been folded on their respective best periods; the unbinned phase-folded points are shown as open symbols.

the 0.01% false-alarm probability (FAP; see Zechmeister & Kürster 2009) level in all bands (shown in Figure 4). The detrended data reveal peaks and troughs with amplitudes in the range of 0.04–0.08 mag across all bands. Motivated by the synchronized behavior of the multiband photometry, we compute a periodogram fitting all the *BgcVroi* photometry simultaneously using the package *gatspy* (VanderPlas & Ivezić 2015; VanderPlas 2016), which generates a Lomb

–Scargle (Scargle 1982) periodogram for a multiband time series (Figure 4). The best period for the combined multiband observations is  $\approx 12.5$  days.

The consistency of the observed periodicity across the time series was verified through empirical mode decomposition (EMD; Huang et al. 1998, 1999), which is ideally suited to oscillatory detections in the presence of nonlinear and nonstationary processes that may impact the light curves of SNe. Following the methodology outlined by Jess et al. (2023), the intrinsic mode functions (IMFs) are extracted from the detrended time series. Subsequently, a Hilbert–Huang transformation (Huang & Wu 2008) was performed to investigate the instantaneous frequencies across the observing window. A low-order IMF exhibits a frequency associated with a  $\approx 12.5$ -day period for the majority of the time series with little variation. Hence, the EMD processes applied here directly and independently support the GLS periodograms depicted in Figure 4.

We recalculate the bolometric light curve using only the *gcoiz* bands to avoid washing out the periodicity with interpolation. Following identical detrending methods to the bolometric light curve, we measure the size of the oscillations (peak to trough) to be  $\sim 2 \times 10^{40}$  erg s $^{-1}$  over the underlying radioactively powered flux, which is on the order of 1% of the peak bolometric luminosity. We perform numerical integration under a single bump in the bolometric light curve to estimate the radiated energy  $E_{\text{rad,bump}} \approx 10^{46}$  ergs.

### 4.3. Spectra

The spectroscopic evolution of SN 2022jli is shown in Figure 2, spanning from  $-53$  days before maximum light to  $+48$  days after. This includes a spectrum during the first maximum, which is unusual for SNe with a short-lived early peak. The line identifications in this section are based on those by Hunter et al. (2009).

The first spectrum obtained during the early excess displays P Cygni absorption features of Na I D  $\lambda\lambda 5891, 5897$  and strong Fe II  $\lambda\lambda 4924, 5018, 5169$  absorption, typical of Type Ic SNe. The broader spectral coverage of the EFOSC2 spectrum ( $-39$  days) reveals Ca II H and K lines and the Ca II near-IR triplet.

The spectra from  $+21.5$  days show the emergence of a Sc II feature and have a complex blend of narrow emission lines and P Cygni features like some interacting SNe. The forbidden [Ca II]  $\lambda\lambda 7291, 7324$  lines are prominent in the later spectra. We measure the velocities using Gaussian fits to the Fe II  $\lambda\lambda 4924, 5018, 5169$  P Cygni absorption troughs as a proxy for the photospheric velocity. At  $-39$  days we measure  $8500 \pm 300$  km s $^{-1}$ ,  $7000 \pm 300$  km s $^{-1}$  at  $+21$  days, reducing further to  $6700 \pm 300$  km s $^{-1}$  by the  $+48$ -day spectrum, representing a slow recession of the photosphere inside the ejecta.

We note the resemblance of the SN 2022jli spectra to SN 1994I but also to SN 2004gk, although the spectroscopic evolution is not analogous to either object. Given the broad complex at H $\alpha$ , which may be contaminated by Si II and C II, we cannot rule out H in the ejecta or CSM shell(s), but from the line ratios of other H lines we expect the contribution of H to be small. We also fail to identify unambiguous signatures of He in the spectra.

We include comparison spectra of two representative Type Ic events, SN 2004gk (Shivvers et al. 2019) and SN 1994I (Modjaz et al. 2014). The post-peak ( $+25$  days) spectrum of SN 2004gk best resembles the  $-39$ -day spectrum of SN 2022jli. This suggests that SN 2022jli has undergone an

unusual evolution to resemble a post-peak normal Type Ic spectrum at this phase.

We produced a TARDIS (Kerzendorf & Sim 2014; Kerzendorf et al. 2023) model (Figure 2) with the aim of reproducing the main spectral features of SN 2022jli during the first EFOSC2 spectrum. The model is a simple uniform abundance model with an H- and He-deficient composition dominated by C, O, Si, and Mg and a photospheric velocity of  $7500$  km s $^{-1}$ . We adopt a  $t_{\text{explosion}}$  parameter (time since the start of homologous expansion) of 42 days before the observation at  $-39$  days to best match the observed features. We successfully reproduce the prominent Fe II and Ca II features and continuum shape and show that a plausible Type Ic SN composition can reproduce the spectrum. The model does not reproduce the bump at  $6500$  Å or the emission at  $6150$  Å. The TARDIS configuration file is available in a .tar.gz package.

## 5. Discussion

The data presented in this paper show that SN 2022jli is unusual in many respects. The duration of the initial excess ( $\gtrsim 25$  days with no constraining nondetection) is unprecedented for a Type Ic SN. The bolometric light curve peaks at least 59 days after explosion and could be longer given the uncertainty in explosion epoch. In combination with the periodic undulations, the SN 2022jli observational data set is unique.

### 5.1. Scenarios for Periodic Variability

#### 5.1.1. Interaction with CSM

The bumps we observe in the light curve could be due to ejecta interacting with concentric shells of circumstellar material. During the undulation, SN 2022jli is overluminous by  $\sim 1 \times 10^{40}$  erg s $^{-1}$  for 12.5 days. Using the scaling relation  $L = \frac{1}{2} M_{\text{CSM}} v^2 / t_{\text{rise}}$  (Smith & McCray 2007; Quimby et al. 2007; Nicholl et al. 2016), we estimate the mass required for each bump to be  $M_{\text{CSM,bump}} \approx 10^{-5} M_{\odot}$ , assuming  $v = 7000$  km s $^{-1}$  from Fe II line velocity measurements, and  $t_{\text{rise}} = 6.3$  days.

The average pre-explosion mass-loss rate needed to produce this CSM mass per undulation can be calculated by setting  $\dot{M}/v_w = M_{\text{CSM,bump}}/\Delta R$ , where  $v_w$  is the wind velocity and  $\Delta R = vt_{\text{bump}}$  is the radial distance bounding this CSM mass. For an SN velocity  $v = 7000$  km s $^{-1}$  and  $t_{\text{bump}} = 12.5$  days, this gives  $\dot{M} \approx \text{few} \times 10^{-5} (v_w/1000 \text{ km s}^{-1}) M_{\odot} \text{ yr}^{-1}$ . This is consistent with the mass-loss rates observed from Wolf–Rayet stars (e.g., Sander & Vink 2020), suggesting that a “typical” wind mass-loss rate could potentially provide the CSM structure needed to explain the periodic undulations of SN 2022jli, if subjected to a periodic modulation.

Nested shells of dust caused by colliding winds in a massive binary system have recently been spectacularly revealed in JWST imaging (Lau et al. 2022). They showed that the 17 observed shells were due to repeated dust formation episodes every 7.93 yr modulated by periastron passage of the companion O5.5fc star in the mutual orbit around the WC7 Wolf–Rayet star. An ejection velocity of  $v = 7000$  km s $^{-1}$  means that the SN shock front travels  $\Delta r \approx 54$  au in 12.5 days. By comparison, the nested dust shells around WR 140 are  $\Delta r = 4380 \pm 120$  au. If SN 2022jli undulations were due to peaks in CSM density similar to WR 140 shells, a binary progenitor would need to eject these shells on timescales  $\sim 100$  times more frequent, or with a  $\sim 0.2$  yr periodicity. We note that the dust emission in the

shells in WR 140 does not necessarily imply enhanced gas densities (Pollock et al. 2021).

In this scenario of concentric shells or rings, one might expect that light-travel time effects could broaden the undulation timescale as the shock expands. As the SN ejecta hits the back and front of the shells at the same time, the light-travel time from the back to front increases as  $\Delta t_{\text{lt}} \simeq 2v_{\text{ej}}t_{\text{exp}}/c$ , or about 9 days (after 200 days of expansion). While there will be an integrated signal from all parts of the shell, the effect should be to broaden the timescale of the undulations; should the ejecta be photospheric, the broadening effect will be less. The data do not clearly support such broadening.

We can explore potential progenitor candidates using the BPASSV2.2 predictions (Eldridge et al. 2017; Stanway & Eldridge 2018), restricting our search to Type Ic progenitors (see Stevance & Eldridge 2021): we select hydrogen-deficient systems with surface mass hydrogen  $<0.0001 M_{\odot}$  and surface hydrogen mass fraction  $<0.01$ . We also restrict our search to helium-depleted SN progenitors, with helium mass fraction  $<0.3$ . We then look for systems that satisfy the period estimate of a WR 140–like scenario by searching for  $P = 0.07 \pm 0.015$  yr (the error is chosen to give a window of roughly  $\pm 5$  days). Finally, we also impose a luminosity and temperature constraint ( $\log(L/L_{\odot}) > 5$  and  $\log(T/T_{\odot}) > 4.3$ ), as we are looking for WR+O star systems. We find 27 BPASS models at solar metallicity that fulfill these requirements, and including the initial mass function weighting, we would expect about 15 such systems to be formed per 1 million  $M_{\odot}$ . All these systems have primary star (SN progenitor) masses in a rather narrow range of 10–13  $M_{\odot}$ , while the secondaries range from 24.5 to 60  $M_{\odot}$ . Although all these predicted systems have stellar winds around  $0.8 \times 10^{-5} M_{\odot} \text{ yr}^{-1}$ , similar to the estimated requirement to create the CSM as mentioned in Section 5.1.1, a key factor in the periodic modulation is the eccentricity of the system. Stellar evolution models such as BPASS assume circularized orbits, so we cannot assess how many systems would be born with and maintain sufficient eccentricity.

### 5.1.2. Accreting Compact Object

An alternative mechanism to produce light-curve bumps in Type Ibc SNe was suggested by Hirai & Podsiadlowski (2022). After an SESN in a binary system, the newly born neutron star (NS) may receive a kick in the favorable direction of its companion. As a result, the NS may penetrate or skim the surface of the binary companion. They predict that material captured from the companion settles around the NS and that the accretion rate is likely to be super-Eddington. The accretion could result in outflows or jets that add further energy to the SN ejecta and result in additional luminosity. Accretion resulting in jets has been modeled by Hober et al. (2022), which they propose could power bumps in the late-time light curves of SNe. Undulations in the light curves of SLSNe have been detected (Nicholl et al. 2016; Inserra et al. 2017; Gomez et al. 2021; Hosseinzadeh et al. 2022; West et al. 2023), but no repeating signature has been confirmed over multiple cycles.

Hirai & Podsiadlowski (2022) calculate that even if only  $\sim 0.01 M_{\odot}$  is captured by the NS and if only  $\sim 1\%$  of that is accreted, then the energy available would be of order  $E_{\text{acc}} \sim M_{\text{acc}}c^2 \sim 10^{50}$  erg, which is comfortably enough to power a few percent of the total integrated SN flux of  $E_{\text{rad}} \simeq 2.5 \times 10^{49}$  erg. The direct interaction invoked in Hirai & Podsiadlowski (2022) requires a fairly fine-tuned kick direction

and velocity. However, a milder interaction as discussed in Hirai et al. (2018) and Ogata et al. (2021) may be sufficient. The companion star is inflated by heating from the SN ejecta –companion interaction, and the inflated part of the envelope may interact with the NS, causing periodic accretion on the timescale of the orbit.

Accretion-powered jets after core collapse also have sufficient energy (Soker 2022; Hober et al. 2022) to power the excess flux observed in the light curve of SN 2022jli, but a modulation process is required. In the Hirai & Podsiadlowski (2022) scenario, the gradual inspiral of the NS into the companion is a pathway for the formation of a Thorne –Żytkow object (TŻO). TŻOs, which are NSs inside an envelope of nondegenerate diffuse material, have been predicted in the literature (Thorne & Żytkow 1975, 1977), but very few real candidates exist (O’Grady et al. 2020). An issue of the Hirai & Podsiadlowski (2022) scenario is that the orbit of the NS will decay rapidly (within  $\sim 5$  orbits), making 15 orbital cycles problematic. However, in the inflated companion case, the low-density envelope results in slower orbital decay (Hirai et al. 2018; Ogata et al. 2021).

The accreting compact object model can be thought of as an internal powering source. The energy released must diffuse out through the ejecta on timescales determined by the opacity, density, and radius of the optically thick material. Hosseinzadeh et al. (2022) propose that a central origin is disfavored if the dimensionless depth of the powering source,  $\delta \simeq \frac{t_{\text{bump}} \Delta t_{\text{bump}}}{t_{\text{rise}}^2}$ , is significantly less than unity. With  $\Delta t_{\text{bump}} \simeq 12.5$  and  $t_{\text{rise}} \simeq 60$ , this parameter then ranges between 0.2 and 0.7 for the earliest and latest bumps. This would marginally disfavor a central, internal powering source, although Hosseinzadeh et al. (2022) note that the expression is quite approximate and should only be treated as an order-of-magnitude result.

## 5.2. Scenarios for Initial Maximum

### 5.2.1. Interaction with CSM

MOSFiT modeling of the early excess with an interaction-powered model requires  $M_{\text{ej}} \approx 12 M_{\odot}$ , which is compatible with the mass required for the long rise to maximum light. However, the duration requires significant  $M_{\text{CSM}}$  ( $>3 M_{\odot}$  in our modeling), which is very large for a Type Ic SN and would require an exotic mechanism to drive extreme mass loss shortly before explosion, such as pulsational pair-instability SN ejections (Woosley 2017).

Perhaps the apparent duration of SCE is extended owing to enhanced opacity caused by Thomson scattering in the CSM (Moriya & Maeda 2012), which is eventually overtaken by the forward shock. Finally, the red spectrum during the first peak (Grzegorzec 2022) would appear inconsistent with luminous circumstellar interaction at early times (i.e., with compact CSM).

We cannot exclude CSM interaction as the source of the early excess; to do so would require more data to constrain the excess or more sophisticated modeling of the interaction to determine the viability of this scenario.

### 5.2.2. Companion Collision

Here we consider the emission from the collision of ejecta with the binary companion of SN 2022jli using the model suggested by Kasen (2010). In this scenario the interaction

shocks the SN ejecta, dissipating kinetic energy causing bright optical/UV emission. This additional contribution to the observed luminosity exceeds the radioactively powered SN for a short period, resulting in an early excess. We investigate the viability of this model using Equations (22) and (23) from (Kasen 2010) to estimate the luminosity and the collision luminosity timescale ( $t_c$ ) where ( $L_{c,iso} > L_{Ni}$ )

$$L_{c,iso} = 10^{43} a_{13} M_c^{1/4} v_9^{7/4} \kappa_e^{-3/4} t_{day}^{-1/2} \text{erg s}^{-1}, \quad (1)$$

$$t_c < 7.3 a_{13}^{2/5} M_c^{1/2} v_9^{3/10} \kappa_e^{1/10} \frac{\kappa_{Ni}}{\kappa_e}^{2/5} M_{Ni,0.6}^{-2/5}, \quad (2)$$

where  $a_{13} = a/10^{13}$  cm ( $a$  is the orbital separation),  $M_c = M/M_{Ch}$  is the ejecta mass  $M$  in units of the Chandrasekhar mass ( $M_{Ch}$ ),  $v_9 = v_t/10^9$  cm s $^{-1}$ ,  $v_t = 6 \times 10^8 \zeta_v (E_{51}/M_c)^{1/2}$  cm s $^{-1}$  (following Kasen 2010, we adopt  $\zeta_v = 1.69$ ),  $\kappa_{Ni}$  is the opacity in the  $^{56}\text{Ni}$ -dominated region, and  $\kappa_e$  is the ejecta opacity outside this region. The time since explosion is given as  $t_{day}$ ,  $M_{Ni,0.6} = M_{Ni}/0.6 M_\odot$ ,  $E_{51} = E/10^{51}$  erg s $^{-1}$ , and  $E$  is the explosion energy. We adopt an indicative ejecta mass of  $12 M_\odot$  from MOSFiT modeling in Section 4.1.2 and set  $\kappa_e = \kappa_{Ni} = 0.1$  cm $^2$  g $^{-1}$ . We set  $M_{Ni} \approx 0.7$  (for  $f_{Ni} \approx 0.06$  from MOSFiT) and set  $v_t = 8500$  km s $^{-1}$  from direct measurement of the  $-29$ -day spectrum (during the early excess).

To produce the observed early luminosity on the order of  $\sim 10^{42}$  erg s $^{-1}$  and timescale of  $\sim 10$  days, we would need to have separation  $\sim 1$  au. For these parameters we calculate  $t_c \lesssim 17.5$  days and  $L_{c,iso} \approx 8 \times 10^{43}$  erg s $^{-1}$  for  $t_d = 2$  days and  $L_{c,iso} \approx 2 \times 10^{42}$  erg s $^{-1}$  for  $t_d = 20$  days.

With these assumptions for separation and ejecta mass, our observations are compatible with the direct collision of the ejecta with the companion star. It is important to note that this scenario requires a favorable viewing angle; Kasen (2010) predicts that the collision should be visible in only  $\sim 10\%$  of cases and that an orbital separation of  $\sim 1$  au at the time of interaction may require the object to be close to pericenter. An important additional qualification of the Kasen (2010) model calculation is the assumption that the companion to the exploding star is filling its Roche lobe, as in a thermonuclear binary star explosion. Therefore, this calculation should be regarded only as an illustrative estimate of the energetics of a companion interaction. The progenitor systems considered in Section 5.1.1 have separations of 0.5 au and upward, which is compatible with the 1 au separation adopted for this calculation, although we note that they are typically not filling their Roche lobe and interacting. Should the excess be powered by companion collision, one might expect to observe late-time H $\alpha$  emission from the companion and at late times observe a surviving but inflated companion star.

## 6. Conclusions

We have presented detailed, multiwavelength, high-cadence observations of the unprecedented Type Ic SN 2022jli. We attribute the long rise to maximum as the signature of a large ejecta mass ( $M_{ej} \approx 12 \pm 6 M_\odot$ ). Future nebular phase spectroscopy may provide an independent estimate of the core mass from the [Ca II] and [O I] line ratios (Fransson & Chevalier 1989).

We provide the first unambiguous detection of periodic behavior in an SN optical light curve, measuring a period of  $\sim 12.5$  days and amplitude  $\sim 1\%$  of the SN maximum light, repeating over a time window of at least  $\sim 200$  days. This could

be explained by discrete episodes of shock heating from interaction with a structured CSM produced through modulated mass loss of the progenitor star in a binary system. We also consider companion–compact object interaction as the energy source but favor a structured CSM.

We also observe a prolonged early excess and consider two scenarios: CSM interaction and ejecta–companion interaction. Based on the methods presented in this work, we cannot distinguish between these two scenarios. A dense CSM shell requires several solar masses of material around the progenitor star, requiring exotic phenomena like pulsational pair instability (Woosley 2017) shortly before explosion. Although only visible in 10% of cases, we cannot rule out ejecta–companion interaction, especially given that binarity is already invoked to explain the periodic undulations. However, this scenario has strict requirements on explosion energy and binary separation.

SN 2022jli is the subject of further study and multi-wavelength observations (Moore et al., in preparation). Late-time high-resolution JWST or Hubble Space Telescope photometry may reveal the origin of the CSM or a surviving, inflated companion star (Liu et al. 2015; Hirai et al. 2018).

## Acknowledgments

We thank the anonymous referee for useful comments. ATLAS is primarily funded through NASA grants NN12AR55G, 80NSSC18K0284, and 80NSSC18K1575. The ATLAS science products are provided by the University of Hawaii, Queen’s University Belfast, STScI, SAAO, and Millennium Institute of Astrophysics in Chile. M.N., S.S., A. A., and X.S. are supported by the European Research Council (ERC) under the European Union’s Horizon 2020 research and innovation program (grant agreement No. 948381) and by UK Space Agency grant No. ST/Y000692/1. Lasair is supported by the UKRI Science and Technology Facilities Council and is a collaboration between the University of Edinburgh (grant ST/N002512/1) and QUB (grant ST/N002520/1) within the LSST:UK Science Consortium. ZTF is supported by National Science Foundation grant AST-1440341 and a collaboration including Caltech, IPAC, the Weizmann Institute for Science, the Oskar Klein Center at Stockholm University, the University of Maryland, the University of Washington, Deutsches Elektronen-Synchrotron and Humboldt University, Los Alamos National Laboratories, the TANGO Consortium of Taiwan, the University of Wisconsin at Milwaukee, and Lawrence Berkeley National Laboratories. This work is based on observations collected at the European Organisation for Astronomical Research in the Southern Hemisphere, Chile, as part of ePESSTO+ (the advanced Public ESO Spectroscopic Survey for Transient Objects Survey). ePESSTO+ observations were obtained under ESO program ID 108.220C (PI: Inserra). The Las Cumbres Observatory (LCO) data have been obtained via an OPTCON proposal (IDs: OPTICON 22A/004, 22B/002; European Union’s Horizon 2020 grant agreement No. 730890), and the LCO team is supported by NSF grants AST-1911225 and AST-1911151. S.S., S.A.S., and S.J.S. acknowledge funding from STFC grants ST/X006506/1 and ST/T000198/1. D.B.J. and S.D.T.G. acknowledge funding from STFC grant awards ST/T00021X/1 and ST/X000923/1. D.B.J. and W.B. acknowledge support from the Leverhulme Trust via the Research Project Grant RPG-2019-371. L.G. and C.P.G. acknowledge financial support from the Spanish Ministerio de Ciencia e Innovación (MCIN), the Agencia

Estatad de Investigaci3n (AEI) 10.13039/501100011033, and the European Social Fund (ESF) ‘‘Investing in your future’’ under the 2019 Ram3n y Cajal program RYC2019-027683-I; the Marie Skłodowska-Curie and the Beatriu de Pin3s 2021 BP 00168 program and the PID2020-115253GA-I00 HOST-FLOWS project, from Centro Superior de Investigaciones Científicas (CSIC) under the PIE project 20215AT016; and the program Unidad de Excelencia María de Maeztu CEX2020-001058-M. We acknowledge funding from ANID, Millennium Science Initiative, ICN12\_009. G.L. is supported by a research grant (19054) from VILLUM FONDEN. T.W.C. thanks the Yushan Young Fellow Program by the Ministry of Education, Taiwan for the financial support.

*Facilities:* NTT, UH:2.2m, PO:1.2m, Liverpool:2m, LCOGT, Gaia, Swift.

*Software:* Astropy (Astropy Collaboration et al. 2013, 2018, 2022), Numpy (Harris et al. 2020), Matplotlib (Guillochon et al. 2018), Mosfit (Guillochon et al. 2018), Hoki (Stevance et al. 2020), PSF (Nicholl et al. 2023).

## Appendix MOSFiT Posterior

We show the posterior distribution in Figure 5 for the  $^{56}\text{Ni}$  model fit to SN 2022jli described in Section 4.1.2.

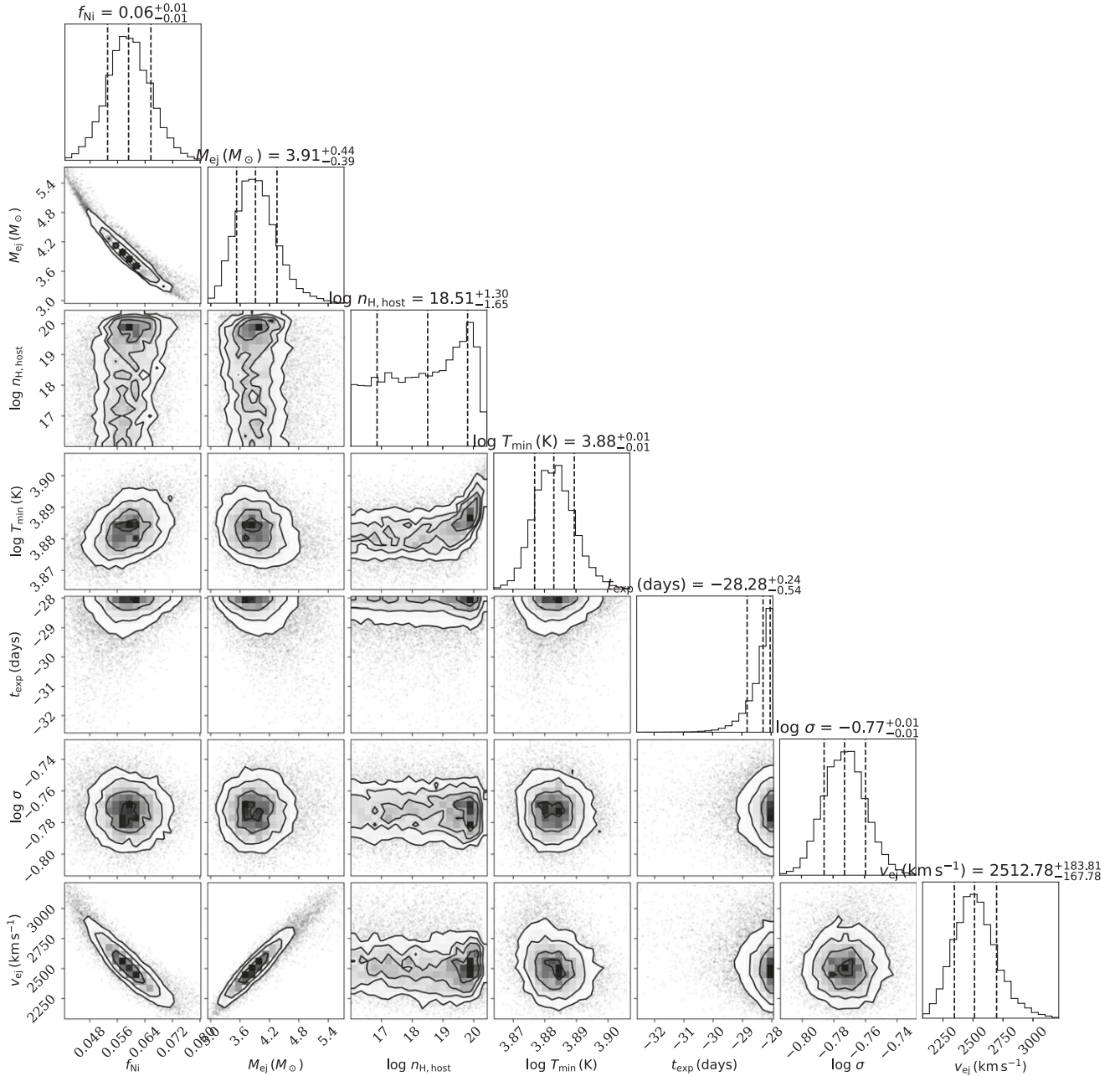


**Figure 5.** Posterior distribution for the physical parameters of the MOSFiT default model fit to SN 2022jli. In this model  $f_{\text{Ni}}$  is the fraction of  $^{56}\text{Ni}$  in the ejecta and  $M_{\text{ej}}$  is the mass in solar masses. Ejecta velocity is  $V_{\text{ej}}$  and  $\log n_{\text{H,host}}$  is the logarithm of the host H column density.  $T_{\text{min}}$  is the temperature floor as defined in Nicholl et al. (2017), and  $t_{\text{exp}}$  determines the explosion epoch relative to the earliest photometry point. The  $\sigma$  parameter is a white-noise parameter that, when added to all data, gives a  $\chi^2$  equal to 1.

## ORCID iDs

T. Moore  <https://orcid.org/0000-0001-8385-3727>  
 S. J. Smartt  <https://orcid.org/0000-0002-8229-1731>  
 M. Nicholl  <https://orcid.org/0000-0002-2555-3192>  
 S. Srivastav  <https://orcid.org/0000-0003-4524-6883>  
 H. F. Stevance  <https://orcid.org/0000-0002-0504-4323>  
 D. B. Jess  <https://orcid.org/0000-0002-9155-8039>  
 S. D. T. Grant  <https://orcid.org/0000-0001-5170-9747>  
 M. D. Fulton  <https://orcid.org/0000-0003-1916-0664>  
 L. Rhodes  <https://orcid.org/0000-0003-2705-4941>  
 S. A. Sim  <https://orcid.org/0000-0002-9774-1192>  
 R. Hirai  <https://orcid.org/0000-0002-8032-8174>  
 P. Podsiadlowski  <https://orcid.org/0000-0002-8338-9677>  
 J. P. Anderson  <https://orcid.org/0000-0003-0227-3451>  
 C. Ashall  <https://orcid.org/0000-0002-5221-7557>  
 W. Bate  <https://orcid.org/0000-0001-9629-5250>  
 R. Fender  <https://orcid.org/0000-0002-5654-2744>  
 C. P. Gutiérrez  <https://orcid.org/0000-0003-2375-2064>  
 D. A. Howell  <https://orcid.org/0000-0003-4253-656X>  
 M. E. Huber  <https://orcid.org/0000-0003-1059-9603>  
 C. Inserra  <https://orcid.org/0000-0002-3968-4409>  
 G. Leloudas  <https://orcid.org/0000-0002-8597-0756>  
 T. E. Müller-Bravo  <https://orcid.org/0000-0003-3939-7167>  
 B. J. Shappee  <https://orcid.org/0000-0003-4631-1149>  
 K. W. Smith  <https://orcid.org/0000-0001-9535-3199>  
 G. Terreran  <https://orcid.org/0000-0003-0794-5982>  
 J. Tonry  <https://orcid.org/0000-0003-2858-9657>  
 M. A. Tucker  <https://orcid.org/0000-0002-2471-8442>  
 D. R. Young  <https://orcid.org/0000-0002-1229-2499>  
 A. Aamer  <https://orcid.org/0000-0002-9085-8187>  
 T.-W. Chen  <https://orcid.org/0000-0002-1066-6098>  
 F. Ragosta  <https://orcid.org/0000-0003-2132-3610>  
 L. Galbany  <https://orcid.org/0000-0002-1296-6887>  
 M. Gromadzki  <https://orcid.org/0000-0002-1650-1518>  
 L. Harvey  <https://orcid.org/0000-0003-3393-9383>  
 P. Hoeflich  <https://orcid.org/0000-0002-4338-6586>  
 C. McCully  <https://orcid.org/0000-0001-5807-7893>  
 M. Newsome  <https://orcid.org/0000-0001-9570-0584>  
 E. P. Gonzalez  <https://orcid.org/0000-0003-0209-9246>  
 C. Pellegrino  <https://orcid.org/0000-0002-7472-1279>  
 P. Ramsden  <https://orcid.org/0009-0009-2627-2884>  
 M. Pérez-Torres  <https://orcid.org/0000-0001-5654-0266>  
 E. J. Ridley  <https://orcid.org/0009-0008-2579-1810>  
 X. Sheng  <https://orcid.org/0000-0002-6527-1368>  
 J. Weston  <https://orcid.org/0009-0002-9460-9900>

## References

Alam, S., Albareti, F. D., Allende Prieto, C., et al. 2015, *ApJS*, 219, 12  
 Anupama, G. C., Sahu, D. K., Deng, J., et al. 2005, *ApJL*, 631, L125  
 Arnett, W. D. 1982, *ApJ*, 253, 785  
 Astropy Collaboration, Price-Whelan, A. M., Lim, P. L., et al. 2022, *ApJ*, 935, 167  
 Astropy Collaboration, Price-Whelan, A. M., Sipőcz, B. M., et al. 2018, *AJ*, 156, 123  
 Astropy Collaboration, Robitaille, T. P., Tollerud, E. J., et al. 2013, *A&A*, 558, A33  
 Bellm, E. C., Kulkarni, S. R., Graham, M. J., et al. 2019, *PASP*, 131, 018002  
 Brennan, S. J., & Fraser, M. 2022, *A&A*, 667, A62  
 Brown, P. J., Holland, S. T., Immler, S., et al. 2009, *AJ*, 137, 4517  
 Brown, T. M., Baliber, N., Bianco, F. B., et al. 2013, *PASP*, 125, 1031  
 Chatzopoulos, E., Wheeler, J. C., Vinko, J., Horvath, Z. L., & Nagy, A. 2013, *ApJ*, 773, 76  
 Cosentino, S. P., Evans, C. R., Parrag, E., et al. 2022, *TNSAN*, 116, 1  
 Eldridge, J. J., Stanway, E. R., Xiao, L., et al. 2017, *PASA*, 34, e058

Fitzpatrick, E. L. 1999, *PASP*, 111, 63  
 Flewelling, H. A., Magnier, E. A., Chambers, K. C., et al. 2020, *ApJS*, 251, 7  
 Fransson, C., & Chevalier, R. A. 1989, *ApJ*, 343, 323  
 Fraser, M., Inserra, C., Jerkstrand, A., et al. 2013, *MNRAS*, 433, 1312  
 Fraser, M., Kotak, R., Pastorello, A., et al. 2015, *MNRAS*, 453, 3886  
 Gaia Collaboration, Prusti, T., de Bruijne, J. H. J., et al. 2016, *A&A*, 595, A1  
 Gal-Yam, A. 2017, in *Handbook of Supernovae*, ed. A. W. Alsabti & P. Murdin (Cham: Springer), 195  
 Gehrels, N., Chincarini, G., Giommi, P., et al. 2004, *ApJ*, 611, 1005  
 Gomez, S., Berger, E., Hosseinzadeh, G., et al. 2021, *ApJ*, 913, 143  
 Grzegorzek, J. 2022, *TNSCR*, 2022-1261, 1  
 Guillochon, J., Nicholl, M., Villar, V. A., et al. 2018, *ApJS*, 236, 6  
 Hachinger, S., Mazzali, P. A., Taubenberger, S., et al. 2012, *MNRAS*, 422, 70  
 Harris, C. R., Millman, K. J., van der Walt, S. J., et al. 2020, *Natur*, 585, 357  
 Hirai, R., & Podsiadlowski, P. 2022, *MNRAS*, 517, 4544  
 Henden, A. A., Templeton, M., Terrell, D., et al. 2016, *yCat*, II/336  
 Hirai, R., Podsiadlowski, P., & Yamada, S. 2018, *ApJ*, 864, 119  
 Hober, O., Bear, E., & Soker, N. 2022, *MNRAS*, 516, 1846  
 Hodgkin, S. T., Harrison, D. L., Breedt, E., et al. 2021, *A&A*, 652, A76  
 Hosseinzadeh, G., Berger, E., Metzger, B. D., et al. 2022, *ApJ*, 933, 14  
 Huang, N. E., Shen, Z., & Long, S. R. 1999, *AnRFM*, 31, 417  
 Huang, N. E., Shen, Z., Long, S. R., et al. 1998, *RSPSA*, 454, 903  
 Huang, N. E., & Wu, Z. 2008, *RvGeo*, 46, RG2006  
 Hunter, D. J., Valenti, S., Kotak, R., et al. 2009, *A&A*, 508, 371  
 Inserra, C., Nicholl, M., Chen, T. W., et al. 2017, *MNRAS*, 468, 4642  
 Jess, D. B., Jafarzadeh, S., Keys, P. H., et al. 2023, *LRSP*, 20, 1  
 Jiang, B., Jiang, S., & Villar, V. A. 2020, *RNAAS*, 4, 16  
 Karamahmetoglu, E., Sollerman, J., Taddia, F., et al. 2023, *A&A*, in press  
 Kasen, D. 2010, *ApJ*, 708, 1025  
 Kerzendorf, W., Sim, S., Vogl, C., et al. 2023, tardis-sn/tardis: TARDIS v2023.08.13, release-2023.08.13, Zenodo, doi:10.5281/zenodo.8244935  
 Kerzendorf, W. E., & Sim, S. A. 2014, *MNRAS*, 440, 387  
 Kochanek, C. S., Shappee, B. J., Stanek, K. Z., et al. 2017, *PASP*, 129, 104502  
 Kuin, N. P. M., Wu, K., Oates, S., et al. 2019, *MNRAS*, 487, 2505  
 Langer, N. 2012, *ARA&A*, 50, 107  
 Lantz, B., Aldering, G., Antilogus, P., et al. 2004, *Proc. SPIE*, 5249, 146  
 Lau, R. M., Hankins, M. J., Han, Y., et al. 2022, *NatAs*, 6, 1308  
 Liu, Z.-W., Tauris, T. M., Röpke, F. K., et al. 2015, *A&A*, 584, A11  
 Lyman, J. D., Bersier, D., James, P. A., et al. 2016, *MNRAS*, 457, 328  
 Margutti, R., Metzger, B. D., Chornock, R., et al. 2019, *ApJ*, 872, 18  
 Martin, J. C., Hamsch, F. J., Margutti, R., et al. 2015, *AJ*, 149, 9  
 Modjaz, M., Blondin, S., Kirshner, R. P., et al. 2014, *AJ*, 147, 99  
 Modjaz, M., Gutiérrez, C. P., & Arcavi, I. 2019, *NatAs*, 3, 717  
 Modjaz, M., Li, W., Butler, N., et al. 2009, *ApJ*, 702, 226  
 Moldon, J., 2021 eMCP: e-MERLIN CASA pipeline, Astrophysics Source Code Library, ascl:2109.006  
 Monard, L. 2022, *TNSCR*, 2022-1198, 1  
 Monard, L. A. G. 2009, *CBET*, 1798, 1  
 Moriya, T. J., & Maeda, K. 2012, *ApJL*, 756, L22  
 Nadyozhin, D. K. 1994, *ApJS*, 92, 527  
 Nicholl, M. 2018, *RNAAS*, 2, 230  
 Nicholl, M., Berger, E., Smartt, S. J., et al. 2016, *ApJ*, 826, 39  
 Nicholl, M., Guillochon, J., & Berger, E. 2017, *ApJ*, 850, 55  
 Nicholl, M., Smartt, S. J., Jerkstrand, A., et al. 2015, *MNRAS*, 452, 3869  
 Nicholl, M., Srivastav, S., Fulton, M. D., et al. 2023, *ApJL*, 954, L28  
 O'Grady, A. J. G., Drout, M. R., Shappee, B. J., et al. 2020, *ApJ*, 901, 135  
 Ogata, M., Hirai, R., & Hijikawa, K. 2021, *MNRAS*, 505, 2485  
 Podsiadlowski, P., Joss, P. C., & Hsu, J. J. L. 1992, *ApJ*, 391, 246  
 Pollock, A. M. T., Corcoran, M. F., Stevens, I. R., et al. 2021, *ApJ*, 923, 191  
 Poznanski, D., Prochaska, J. X., & Bloom, J. S. 2012, *MNRAS*, 426, 1465  
 Prentice, S. J., Ashall, C., James, P. A., et al. 2019, *MNRAS*, 485, 1559  
 Quimby, R. M., Aldering, G., Wheeler, J. C., et al. 2007, *ApJL*, 668, L99  
 Rivera Sandoval, L. E., Maccarone, T. J., Corsi, A., et al. 2018, *MNRAS*, 480, L146  
 Roming, P. W. A., Kennedy, T. E., Mason, K. O., et al. 2005, *SSRv*, 120, 95  
 Ryder, S. D., Sadler, E. M., Subrahmanyam, R., et al. 2004, *MNRAS*, 349, 1093  
 Sander, A. A. C., & Vink, J. S. 2020, *MNRAS*, 499, 873  
 Scargle, J. D. 1982, *ApJ*, 263, 835  
 Schlafly, E. F., & Finkbeiner, D. P. 2011, *ApJ*, 737, 103  
 Shappee, B. J., Prieto, J. L., Grupe, D., et al. 2014, *ApJ*, 788, 48  
 Shenar, T., Gilkis, A., Vink, J. S., Sana, H., & Sander, A. A. C. 2020, *A&A*, 634, A79  
 Shingles, L., Smith, K. W., Young, D. R., et al. 2021, *TNSAN*, 7, 1  
 Shivvers, I., Filippenko, A. V., Silverman, J. M., et al. 2019, *MNRAS*, 482, 1545  
 Smartt, S. J. 2009, *ARA&A*, 47, 63

- Smartt, S. J., Valenti, S., Fraser, M., et al. 2015, *A&A*, **579**, A40
- Smith, K. W., Smartt, S. J., Young, D. R., et al. 2020, *PASP*, **132**, 085002
- Smith, K. W., Williams, R. D., Young, D. R., et al. 2019, *RNAAS*, **3**, 26
- Smith, N., & McCray, R. 2007, *ApJL*, **671**, L17
- Snodgrass, C., Saviane, I., Monaco, L., & Sinclaire, P. 2008, *Msngr*, **132**, 18
- Soderberg, A. M., Berger, E., Page, K. L., et al. 2008, *Natur*, **453**, 469
- Soker, N. 2022, *ApJ*, **935**, 108
- Speagle, J. S. 2020, *MNRAS*, **493**, 3132
- Stanway, E. R., & Eldridge, J. J. 2018, *MNRAS*, **479**, 75
- Steele, I. A., Smith, R. J., Rees, P. C., et al. 2004, *Proc. SPIE*, **5489**, 679
- Stevance, H., Eldridge, J., & Stanway, E. 2020, *JOSS*, **5**, 1987
- Stevance, H. F., & Eldridge, J. J. 2021, *MNRAS*, **504**, L51
- Stritzinger, M., Mazzali, P., Phillips, M. M., et al. 2009, *ApJ*, **696**, 713
- Taddia, F., Fremling, C., Sollerman, J., et al. 2016, *A&A*, **592**, A89
- Taddia, F., Sollerman, J., Fremling, C., et al. 2018, *A&A*, **609**, A106
- Terry, J. N., Paturel, G., & Ekholm, T. 2002, *A&A*, **393**, 57
- Thorne, K. S., & Zytlow, A. N. 1975, *ApJL*, **199**, L19
- Thorne, K. S., & Zytlow, A. N. 1977, *ApJ*, **212**, 832
- Tonry, J. L., Denneau, L., Flewelling, H., et al. 2018a, *ApJ*, **867**, 105
- Tonry, J. L., Denneau, L., Heinze, A. N., et al. 2018b, *PASP*, **130**, 064505
- Tucker, M. A., Shappee, B. J., Huber, M. E., et al. 2022, *PASP*, **134**, 124502
- Tully, R. B., Courtois, H. M., Dolphin, A. E., et al. 2013, *AJ*, **146**, 86
- VanderPlas, J., 2016 gatspy: General tools for Astronomical Time Series in Python, Astrophysics Source Code Library, ascl:1610.007
- VanderPlas, J. T., & Ivezić, Ž. 2015, *ApJ*, **812**, 18
- Villar, V. A., Berger, E., Metzger, B. D., & Guillochon, J. 2017, *ApJ*, **849**, 70
- Vink, J. S., & de Koter, A. 2005, *A&A*, **442**, 587
- Weiler, K. W., van Dyk, S. D., Pringle, J. E., & Panagia, N. 1992, *ApJ*, **399**, 672
- West, S. L., Lunnan, R., Omand, C. M. B., et al. 2023, *A&A*, **670**, A7
- Williamson, M., Kerzendorf, W., & Modjaz, M. 2021, *ApJ*, **908**, 150
- Wilson, R. N. 1983, in European Southern Observatory Conf. and Workshop Proc., The Very Large Telescope project., The NTT (New Technology Telescope) - Predecessor of the VLT, 17, ed. J. P. Swings & K. Kjaer, 173
- Woosley, S. E. 2017, *ApJ*, **836**, 244
- Woosley, S. E., Pinto, P. A., & Hartmann, D. 1989, *ApJ*, **346**, 395
- Yaron, O., & Gal-Yam, A. 2012, *PASP*, **124**, 668
- Zechmeister, M., & Kürster, M. 2009, *A&A*, **496**, 577